Joining by forming technology for thermal applications: A case study of finned tube heat exchanger

Case Studies in Thermal Engineering 59 (2024) 104551

Contents lists available at ScienceDirect

Case Studies in Thermal Engineering

journal homepage: www.elsevier.com/locate/csite

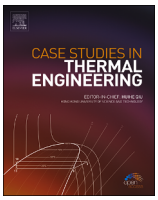

Joining by forming technology for thermal applications: A case study of finned tube heat exchanger

Riccardo Saltarelli [a], Luís M. Alves [b], Matteo Fasano [a, *], Rafael M. Afonso [b, c, **]

[a] Dipartimento Energia, Politecnico di Torino, Corso Duca Degli Abruzzi 24, 10129, Torino, Italy
[b] IDMEC, Instituto Superior Técnico, University of Lisbon, Av. Rovisco Pais, 1049-001, Lisbon, Portugal
[c] Atlântica, Instituto Universitário, Fábrica de Pólvora de Barcarena, 2730-036 Barcarena, Portugal

ARTICLE INFO

Handling Editor: Huihe Qiu

Keywords:
Heat exchanger
Thermal optimization
CFD analysis
Joining by forming
Mechanical joints

ABSTRACT

Heat exchangers are essential for various thermal applications, and their performance could be improved by optimization of layout/operating conditions or materials. The layout/operating conditions optimization has been widely subjected to research and development, while the implementation of different materials has been limited to the available joining solutions. Joining by forming allows to circumvent the existent limitations, since it utilizes plastic deformation to produce multi-material mechanical joints between thin sheets and thin-walled tubes. Here, joining by forming is adopted for the first time, to manufacture multi-material transversal finned tube heat exchangers. The numerical-experimental analysis explores the production of tube compression beads obtained by plastic instability to fix and support fins, and therefore manufacture a novel design of finned heat exchanger with improved performance. A case study is carried out with the help of computational fluid dynamics simulations to find an optimal layout. Then, finite element simulations are employed to analyse the joining by forming process. A prototype model of transversal finned tube heat exchangers was finally manufactured and experimentally tested. Results show considerable gains in comparison with conventional finned tube heat exchangers made from steel tubes and fins, being the multi-material heat exchanger effectiveness doubled with respect to traditional designs.

1. Introduction

The production of compact finned tube heat exchangers comprises the joining of tubes and fins of different configurations and sizes [1–3]. These parts that are found inside the shell structure are commonly joined with fusion welding processes that rely on the development of weld seams by means of gas tungsten arc welding (GTAW) performed with automated orbital welding machines [4,5]. The drawbacks of this joining technology are not only found for its productivity, cost, and inspection requirements, but also due to the distortions and microstructural problems resulting from the heating and cooling cycles of welding, as well as the limitations when dissimilar material connections are to be welded. The latter presents a critical limiting factor for the thermal efficiency of the heat exchanger and compromises its evolution.

To join the different arrays of orthogonal fins to the inner tube, mechanical expansion by means of hydraulic, mechanical, or explosive pressure [5–10] is commonly utilized to expand the tubes against the fins and produce force-fit joints (or interference-fit joints), that are built upon the residual normal stresses (pressures) created between the contact interfaces after tool unloading. This

* Corresponding author.
** Corresponding author.
E-mail addresses: matteo.fasano@polito.it (M. Fasano), rafael.afonso@tecnico.ulisboa.pt, rafonso@uatlantica.pt (R.M. Afonso).

https://doi.org/10.1016/j.csite.2024.104551
Received 5 February 2024; Received in revised form 5 May 2024; Accepted 13 May 2024
Available online 14 May 2024

joining by forming process is carried out at ambient temperature but, to ensure the robustness and leak tightness of the assembly, it is still frequently combined with seal welds made by GTAW [5]. Another joining by forming alternative was already developed for attaching tubes to fins that combines flaring of the free tube end with indentation of the fin by pressing the tube flange against its surface [11]. The mechanical joint results from the combination of force and form-fit mechanisms, in which the latter is obtained from the mechanical interlocking created between the tube and fin [12]. This joining solution can be applied to different material combinations [13,14], however it is limited to the tube ends and therefore to the outer fins.

The objective of this work is to propose and evaluate the utilization of joining by axial tube compression instability [15] to produce joints between a tube and an array of orthogonal fins made from different materials than that of the tube, with the aim to enhance heat exchange efficiency while reducing manufacturing costs. To produce this mechanical joint, a tube is axially compressed while leaving a gap in-between the upper and lower dies that support the tube externally, while a mandrel placed inside the tube avoids inward material flow (leftmost side of Fig. 1a). Along the deformation, the tube collapses under local buckling and gives rise to an axisymmetric compression bead at the gap opening (rightmost side of Fig. 1a). Then, the fin is placed on top of that compression bead (leftmost side of Fig. 1b) and the compression of the free tube end is again repeated to allow the production of another compression bead that will lock the two geometries together (rightmost side of Fig. 1b). To join additional fins to the same tube, the process is repeated several times until all the fins are attached (Fig. 1c).

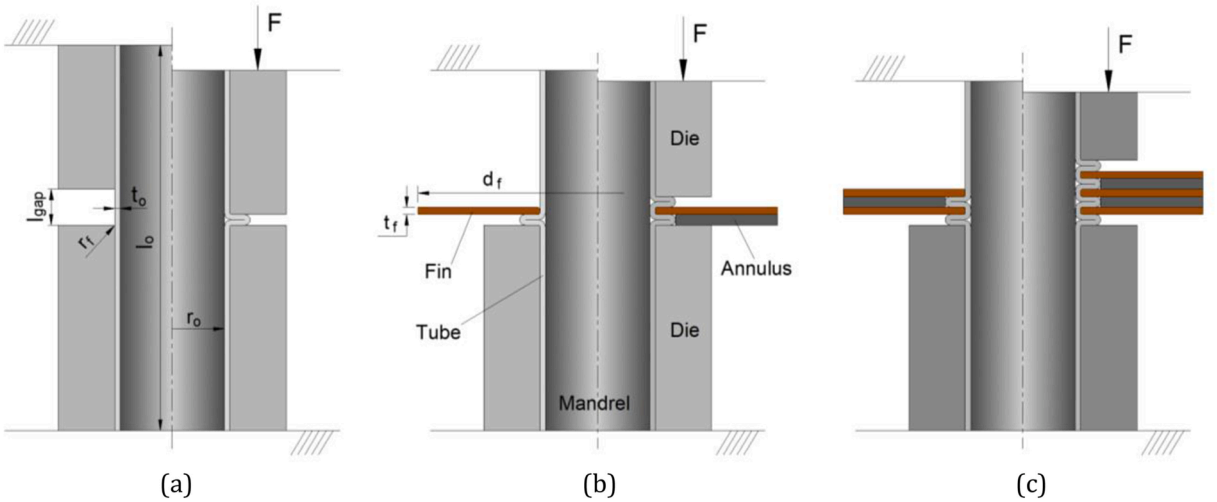

Fig. 1. Schematic representation of (a) axial tube compression instability and (b) subsequent joining of that tube to a single fin and (c) to an array of three fins.

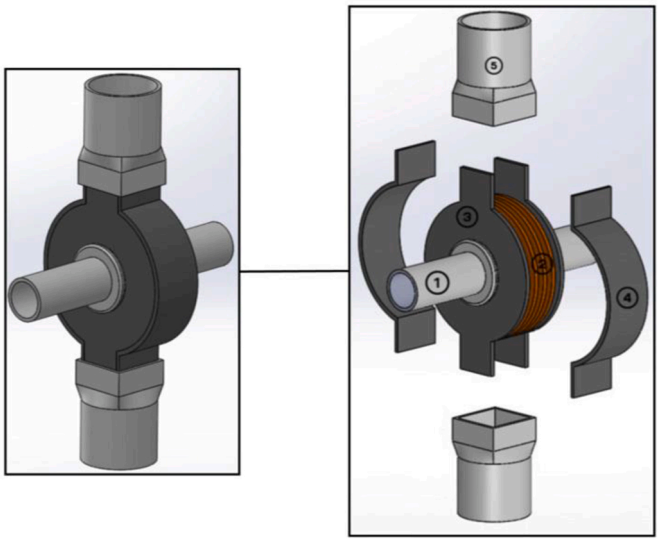

Fig. 2. Schematic of the prototype heat exchanger composed of the inner aluminium tube (1), three central copper fins (2), two outer steel fins (3) that are part of the shell structure along with the two lateral panels (4) and the two square-to-round inlet/outlet attachments (5).

The unique possibility of joining by forming to attach different materials while keeping negligible contact thermal resistance at their interface is crucial to unlock a new class of heat exchangers with additional design freedom. A good case study is the joining of tubes or pipes with lower thermal conductivity (but high mechanical strength and low cost, such as steel tubes or pipes) to fins with enhanced thermal properties (but lower mechanical strength and higher cost, such as copper fins). Following the typical procedure for the design of a heat exchanger, different aspects will be evaluated such as thermal performance, pressure drops, manufacturing feasibility and weight savings.

To choose the layout that optimizes the thermal performance, parametric Computational Fluid Dynamics (CFD) analysis was carried out and then, finite element simulations were employed to predict the plastic deformation mechanisms that govern the joining by forming process. With these results, a prototype of finned tube heat exchanger was manufactured and preliminarily tested to confirm the performance of the new joining approach and validate the CFD simulations for the experimental testing conditions.

2. Materials and methods

2.1. Material characterization

Since the utilization of joining by forming opens the possibility of producing dissimilar material combinations, aluminium tubes AW6063-T6 were joined to 99.9 % electrolytic copper fins, while the outer shell structure was made from steel DC04 (low carbon, cold rolled). This choice of materials was motivated by the need to maximize the thermal conductivity and thus fin efficiency, which justifies the utilization of copper despite its cost and density, and at the same time, the utilization of aluminium is justified not only due to its good formability, but also to balance the weight and cost of the overall assembly, while ensuring good heat exchange properties. For the outer case, the utilization of steel allows to approach the ideal adiabatic conditions defined in the parametric CFD simulations (practical implementations of the heat exchanger assembly would include an additional outer layer of thermal insulation).

The mechanical characterization of the materials was performed by means of tensile tests in accordance with the ASTM standard E8/E8M – 16 and stack compression tests. The latter tests allow to obtain the material stress-strain response for values of strain larger than those obtained in tensile tests. The average flow curves obtained with the hydraulic testing machine Instron SATEC 1200 kN at ambient temperature and with a crosshead speed of 10 mm/min are presented in Supplementary Fig. S1.

2.2. Prototype design and testing

The heat exchanger development started with the selection of the different geometries. Aluminium tubes with an initial length l_0 of 100 mm, a wall thickness t_0 of 1.5 mm and an external radius r_0 of 8 mm were selected, and copper fins of different diameters d_f and thicknesses t_f were subjected to several CFD simulations to identify the most suitable combination of parameters. The outer steel case was obtained from sheet panels with a thickness t of 2 mm and the lateral panels were formed to the required shape.

As for the dies, the range of values of the initial gap opening l_{gap} between the dies and the radius r_f was retrieved from a previous work [15], where the development of plastic instability waves at tubes with the same dimensions was investigated. The values of the previous parameters that were analysed to identify the suitable combination that allows to obtain sound compression beads necessary to support and lock the fins are listed in Table 1.

After the identification of the suitable parameters, the joining process was carried out sequentially until the desired number of fins is attached. Steel mandrels were placed not only inside the tube, but also in-between the fins before each joining operation to avoid deformation of the previously joined fins (refer to Fig. 1c). Then, the outer case was supported by an inlet and outlet aluminium tube. The prototyped heat exchanger as case study is depicted in Fig. 2.

To assess the thermal performance of the prototype heat exchanger, a thermal camera FLIR E86 24° and VALEX P4500 thermocouples were employed, the latter being used to measure the temperature differences of a water flow displaced from the inlet to the outlet of the aluminium tube.

2.3. Parametric CFD analysis

To obtain the optimal combination between the fin external diameter and thickness, nine combinations of these parameters were evaluated with the numerical software ANSYS Fluent®. Those nine layouts were obtained through the combination of each three fin thicknesses of 0.5 mm, 1.5 mm, and 3 mm with each three fin diameters of 40 mm, 60 mm, and 80 mm. The resulting nine configurations were then simulated, and comparisons made to identify the optimal choice.

Starting from nine simplified parametric CAD models defined as shown in Fig. 3a, the CFD computational domain considered the air volume in the heat exchanger (between the outer case and the finned tube) and the finned tube itself, as depicted in Fig. 3b. To reduce the computational effort, both the outer case and the water volume (that was supposed to flow inside the finned tube) were considered as boundary conditions. Accordingly with Fig. 3b, a boundary condition of null heat flux (homogeneous Neumann) was assigned to the external surface indicated with an orange color, a ‘velocity-inlet’ condition on the inlet surface of the air volume

Table 1
Main parameters (see Fig. 1) for the numerical and experimental analysis of the tube-fins system.

Tube			Fins		Dies	
r_0 (mm)	t_0 (mm)	l_0 (mm)	d_f (mm)	t_f (mm)	l_{gap} (mm)	r_f (mm)
16	1.5	100	40, 60, 80	0.5, 1.5, 3	10–15	1.25

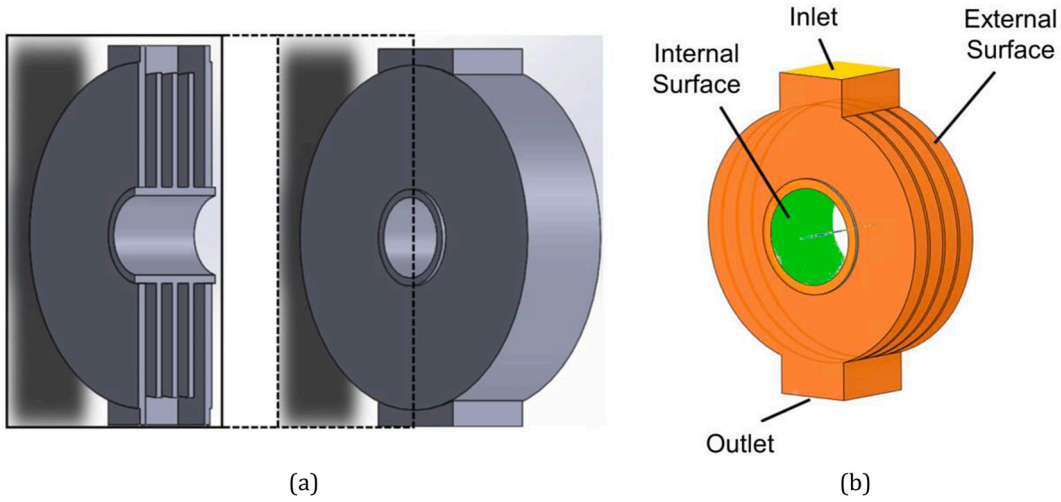

Fig. 3. Comparison between (a) the CAD parametric model and (b) the CFD domain considered, which comprises the tube-fins system and the air volume between the finned tube and the outer case.

(marked with a yellow color), and a 'convection' (Robin) and 'outflow' condition to the internal surface (highlighted with a green color) and outlet surface, respectively. It is worth noting that, in joining by forming processes, parts are joined by plastic deformation and a very tight, continuous contact area is achieved (see the inset in Fig. 4). This leads to negligible values of tube-fin contact thermal resistance [16].

For the convection condition on the internal surface, a heat transfer coefficient of 5000 W/m^{2}K and a free stream temperature of 293 K were chosen as realistic values for the typical conditions of water flowing in a tube of similar dimensions. For the inlet, since its dimensions were proportional to the size of the assembly and therefore dependent on the fin diameter and thickness, different velocities were calculated according to the requirement of a constant Reynolds number and provided as boundary conditions. The inlet air temperature was kept constant at 1000 K.

To close the problem, a 'realizable k-ε' pressure-velocity coupling method with 'enhanced wall treatment' was chosen [17]. A 'SIMPLE' scheme with 'pseudo time steps' option enabled and a Courant number of 2 were selected. Further details on the implemented numerical model are available in the Supplementary Note 1.

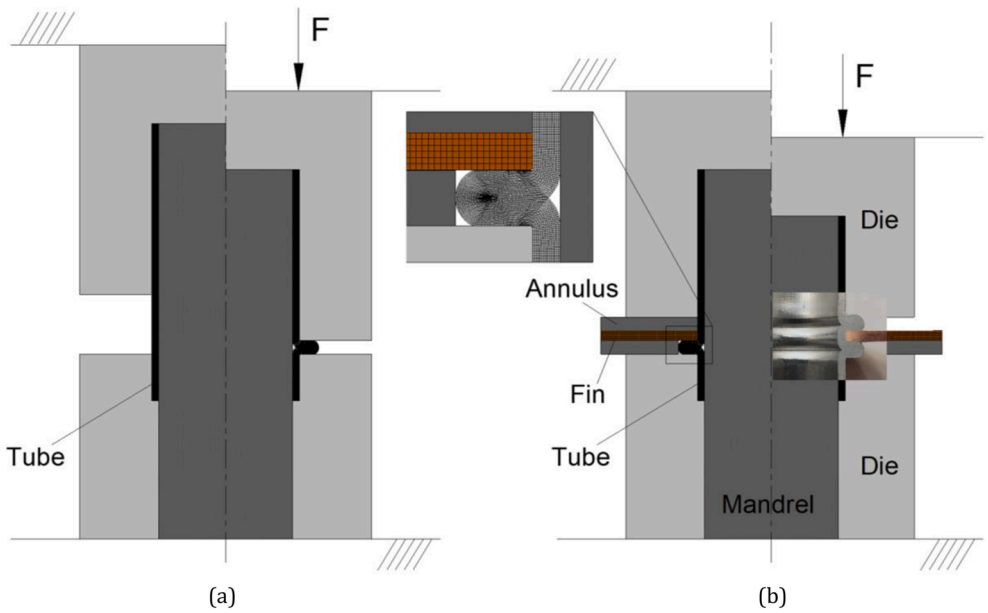

Fig. 4. Finite element model at the (a) initial and (b) final stages of the joining process. A photograph of the cross-section of the tube-fin joint is included in the (b) schematic.

The mesh size was chosen based on a convergence and mesh independence study [18]. The mean outlet air temperature and the heat flux exchanged along the inner tube surface were the controlled variables, calculated for different element sizes. As seen in Supplementary Fig. S2, an element size below 0.4 mm was enough to guarantee mesh-independent results.

With these assumptions, the results of the simulations were collected, and the main thermal fluid dynamics quantities extracted for assessing the heat exchanger performance. The mean outlet air temperature and pressure were calculated averaging the air temperature and pressure over the fluid flow. The exchanged heat flow rate was calculated as the integral over the inner tube surface, representing the heat transmitted to the water. The mass of the metallic parts was calculated multiplying their volumes (measured on the CAD models) by the density of the respective materials. The Nusselt number of air flow was computed considering the middle section between the inlet and outlet ports, being parallel to those sections and crossing the assembly at the maximum fin diameter. The effectiveness ε of the heat exchanger was then computed according to the $\varepsilon - NTU$ method [19], as the ratio between the heat flow rate actually exchanged (Q) and the maximum heat flow rate exchangeable in those same conditions (Q_{max}), namely $\varepsilon = \frac{Q}{Q_{max}}$. The effectiveness gives a direct evaluation of the overall quality of the heat exchanger design, quantifying how close to the ideal target situation the real case is. While Q is estimated by the simulations, the ideal one is computed as: $Q_{max} = C_{min}\ (T_{hot,in} - T_{cold,in})$, where C_{min} is the smallest between $C_{cold} = \dot{m}_{cold} C_{p,cold}$ and $C_{hot} = \dot{m}_{hot} C_{p,hot}$, the subscript "hot" refers to the fluid at higher temperature while "cold" to that at lower temperature, and the subscript "in" to the inlet conditions. As the considered heat transfer fluids were water and air, C_{min} was calculated at the air side for each configuration. $T_{hot,in}$ and $T_{cold,in}$ were imposed by the inlet boundary conditions.

2.4. Numerical prediction of the joining process

The operating conditions for the development of plastic instability and subsequent joining process were numerically modelled with the software i-form [20], which is based on the quasi-static finite element flow formulation and accounts for the contact and sliding with friction between deformable and rigid objects.

Considering the rotational symmetry of the tube and fins, the initial cross-sections of the preforms were discretized by means of axisymmetric quadrilateral elements as seen in Fig. 4. While the numerical evaluation considered the tube and fins as deformable isotropic objects, the dies were modelled as rigid objects and their contours discretized by means of linear contact-friction elements. After the end of each compression beading stage and due to the progressive distortion of the tubular mesh, large local deformations are generated and a remeshing procedure consisting of a global remeshing of the entire deformed object was performed with appropriate transfer of field variables.

To analyse the plastic deformation, friction was modelled with a law of constant friction $\tau_f = mk$, where k is the flow shear strength friction and the friction factor m on the contact interfaces between the dies and objects was selected as 0.1, since it was verified that for this condition, the predicted numerical evolutions presented a good correlation with the experimental results.

3. Results and discussion

3.1. Analysis of the plastic deformation

The first stage of the joining process to produce the compression beading of the thin-walled tube is based on a local buckling collapse mechanism that forces material to flow outward and, eventually, inward if no mandrel was introduced. The numerical analysis performed in i-form for different gaps between the upper and lower dies revealed that the development of a full plastic instability wave is triggered for a gap of 13 mm. Fig. 5a shows the start of plastic instability until a complete compression bead is fully formed (refer to Fig. 5b). Wider gaps will also be able to develop this compression beads but will demand an unnecessary amount of tube material.

After the definition of the ideal gap between the dies, a copper fin was positioned in the surface of the compression bead and a secondary instability wave was produced by tube compression with the same tool system and the introduction of a steel annulus (Fig. 5c). The gap selected was the same as before plus the thickness of the fin that was now introduced. The results allow to verify a uni-

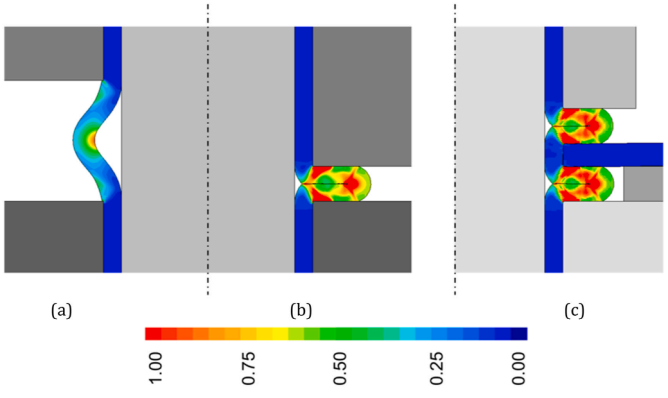

Fig. 5. Computed distribution of effective strain: (a) during the development of a plastic instability wave, (b) after a compression bead is formed and (c) after the joining operation of a single copper fin to an aluminium tube is completed with the development of another locking compression bead.

form contact without empty spaces in-between the fins and the tube compression beads, which is a necessary requirement to guarantee a proper heat conduction between the materials. For the tested conditions, the levels of deformation at the tube compression bead are not significantly modified by the introduction of the fin and the formation of new plastic instability waves (Fig. 5b and c).

Overall, the effective strain distribution allows to conclude that the material becomes strain hardened after the first compression stage (Fig. 5b) and, therefore, that the tube material at the compression bead region after the initial deformation will be able to offer higher resistance to a subsequent deformation that is necessary to join the fin. At each stage, the tube material will increase its resistance with the plastic deformation, which justifies the slight increment in the force of the final compression evolution at the initial stages of the operation, in comparison with the initial compression (refer to Fig. 6). To join additional fins to the same tube and control the deformation of the previously joined fins, a steel annulus needs to be introduced between the fins as it will be described in detail at a later section. It is worth mentioning that squeezing each compression bead even further – to create a larger contact surface that will improve the heat exchange – may result in the development of cracks in the compression bead or excessive deformation of the fin.

The analysis of the force-displacement evolutions in Fig. 6 allows to observe a typical behaviour of a plastic instability mode for the initial stage of the joining process, where the force starts to increase as the tube is axially compressed, until a point where a critical instability load is reached and the force decays slightly as the compression bead is formed. Then, after the fin is positioned in the top of the plastic instability wave, the process is repeated with a final compression, and the previous trend is observed until a sharp rise in the force is verified, as the lower and upper tube beads make full contact with the fin and the joining process is completed.

Here, fin spacing was not considered as a free parameter to be optimized, since its dimension is constrained by the tube thickness in joining by forming processes. More specifically, the axial compression of the tube creates the instability beads used to join the fins with the tube. Therefore, the instability bead – and thus fin spacing – has a thickness equal to two times the tube thickness, as it can be seen in Fig. 6. As a result, the fin spacing is not an independent parameter, being dependent on the tube thickness instead. The latter was not varied in this work since different tube thickness would require the re-optimization of processing parameters for the joining by forming process, which should be done on a case-by-case basis.

3.2. Thermal assessment

For the thermal analysis, a proper definition of the working parameters was required. From the joining process parameters identified in the previous section, the CFD analysis focused on the thickness (t_f) and external diameter (d_f) of the copper fins, while the remaining parameters were kept constant. The heat flow rate exchanged (Q), air pressure drops (ΔP), metallic mass, and the effectiveness of heat exchanger (ε) were assessed for the nine different layouts and compared to a plain tube without fins. This allowed to get reference values that are available from common literature for a plain tube (see Supplementary Note 2 for a model validation with well-established semi-empirical correlations for such configuration without fins) and highlight the gains that come from the introduction of fins.

In both Figs. 7 and 8, the chosen inlet air temperature was 1000 K. For the fluid dynamics conditions, rather than keeping the mass flow rate or the velocity constant, it has been chosen to lock the Reynold number (Re) and computing the corresponding air velocity. The reason is that the Nusselt number (Nu) and, ultimately, the convective heat transfer coefficient (h) both derive from Re rather than fluid velocity alone. A case study value of Re $=$ 600 was then set in all configurations tested in Figs. 7 and 8 (see Supplementary Note 3 for details).

From the relation of Q with the fin diameter and thickness presented in Fig. 7a, it is seen – in comparison with a plain tube – that the introduction of the fins produces a considerable increase in the heat exchange. All the three fin thicknesses share the same trend, although higher values of Q are shown for thicker fins. As the diameter increases, the heat flow rate exchanged rises consistently up to a fin diameter of 60 mm, after which the growth becomes less relevant. For this reason, the utilization of a fin diameter of 80 mm does not justify the increase in weight of the joined assembly (at least for the explored range of geometrical and fluid dynamic parameters).

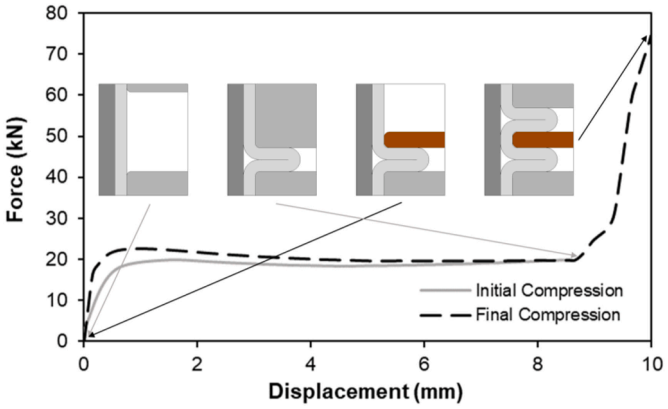

Fig. 6. Experimental force-displacement evolutions to produce an initial tube compression bead and a final tube compression bead for the joining of a single copper fin (with a diameter of 60 mm and a thickness of 2 mm) to the aluminium tube.

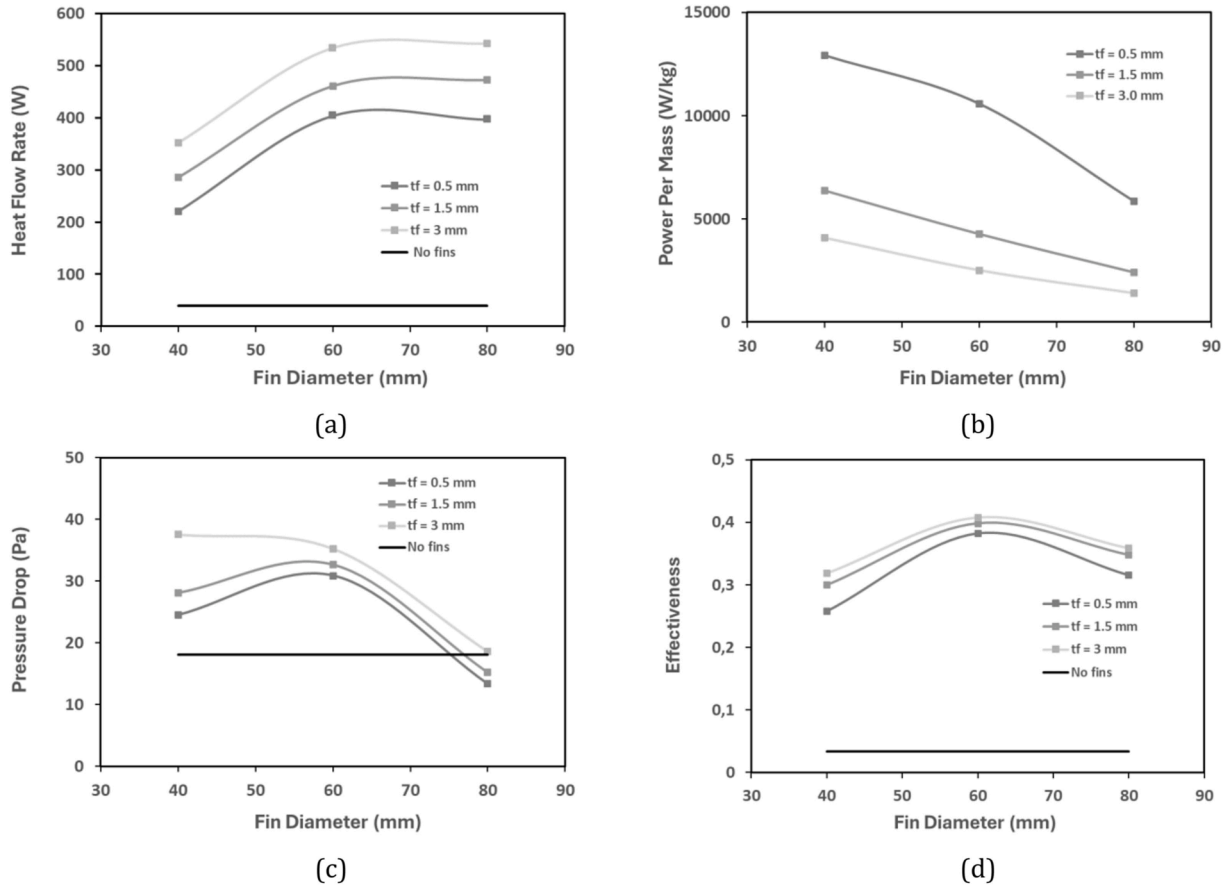

Fig. 7. (a) Evolution of the heat flow rate exchanged Q with the fin diameter D_f and thickness t_f. (b) Evolution of the heat power per mass with the fin diameter and thickness. Such power per mass was calculated by the ratio between the heat flow rate exchanged and the weight of the joined assembly. (c) Evolution of the air pressure drops and of (d) the effectiveness ε of the heat exchanger with the fin diameter and thickness. The plain tube without fins is utilized for reference purposes in both graphs, being independent from fin diameter and thickness values.

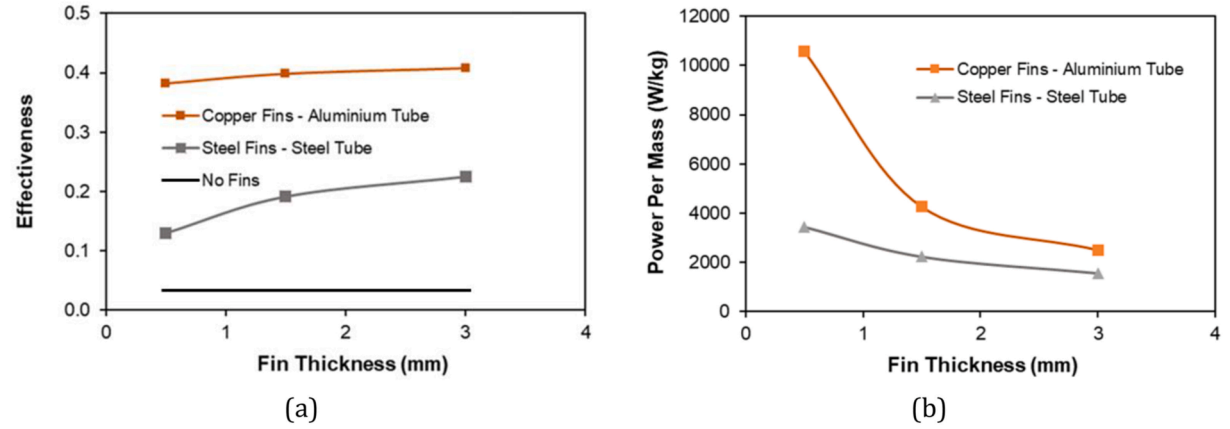

Fig. 8. Evolution of (a) the effectiveness ε and (b) the thermal power per mass with the fin diameter and thickness for different material combinations. The plain tube without fins is utilized for reference purposes in (a).

To quantify the relation between the thermal power and the weight of the structure, their ratio was plotted in Fig. 7b for the different fin diameters and thicknesses tested. The value of this ratio decreases as the fin diameter and thickness are increased, which again suggests a detrimental effect of larger dimensions.

Another important consideration concerns the air pressure drop evolution observed for the different numerical models of the joined assembly that are presented in Fig. 7c. Unlike the previous thermal analysis, the utilization of a diameter of 60 mm presents

lower fluid dynamic performance. However, the absolute values of the pressure drop among the considered layouts appear to be negligible from the practical point of view. Therefore, the optimal fin dimensions have been chosen based on thermal considerations only.

Finally, the effectiveness ε has been computed, which provides an overall view on the quality of the design of the heat exchanger, because it describes how far it is from the maximum thermal performance attainable. As seen in Fig. 7d, ε shows a clear peak for a fin diameter of 60 mm, while being less sensitive to fin thickness.

Considering these CFD analyses, the best configuration for the fins among the considered layouts was achieved for an external diameter of 60 mm. For what concerns the fin thickness, better ε was observed with higher thicknesses, with limited differences between 1.5 mm and 3 mm thickness. Therefore, to avoid excessive weight and reduce pressure drops, a fin thickness of 2 mm was selected for the manufacturing and experimentation of the prototype heat exchanger joined by forming. Notice that the compression beads of the inner tube after joining by forming have not been explicitly modelled in these CFD simulations, since their geometry cannot be defined *a priori* for the different fin thicknesses considered. Nevertheless, a comparative analysis carried out for the best performing case (i.e., 60 mm diameter and 2 mm thickness fins) demonstrates that the discrepancies between configurations with or without compression beads are lower than 5 % in terms of both pressure losses and outlet mean air temperature.

To justify the utilization of multiple materials during manufacturing, namely copper fins, and an aluminium tube, a CFD comparison was carried out with a conventional steel tube and fins assembly with the same (optimal) diameter of 60 mm. The results of effectiveness of Fig. 8a allow to conclude that the utilization of copper fins and an aluminium tube shows better thermal performances for all the three tested fin thicknesses. When the effect of the weight of the tube-fin assembly is considered, the gains in performance become less noticeable for larger fin thicknesses (Fig. 8b), although the enhanced heat transferred still compensates the increased weight introduced by the fins when they are made from copper. These differences become more significant as the fin thickness decreases, where the advantages that come from the utilization of copper fins are more evident.

3.3. Experimental testing

After the numerical analysis performed on a simplified model, a complete prototype was manufactured considering the optimal design of the heat exchanger identified (see Supplementary Fig. S3). This prototype included the mechanical connection between the aluminium tube and three copper fins that are the core of the prototype heat exchanger, as well as two steel fins that work as an outer case together with two semi-circular lateral outer cases that are kept in position by the square-round section aluminium tubes.

Such prototype was preliminarily tested with the objective of validating the CFD simulations, without the intention of reproducing the actual operating conditions of the heat exchanger. Hence, a controlled mass flow rate of hot water was flowed through the inner tube, whereas the outer cases were removed to facilitate natural convection with the surrounding environment. The tests were carried out at a controlled ambient temperature of 28 °C and relative humidity of 70 %. During these characterization tests, the assembly was positioned with its axis vertical and, with the help of two rubber connections placed at the edges of the aluminium joined tube, the water flow was directed and guided along the tube from the bottom to the top as depicted in Fig. 9.

This natural convection test consisted in evaluating the heat exchange performance when the prototype was exposed to the room air and hot water was flowing through the inner tube at a controlled temperature of 60 °C and mass flow rate of 0.142 kg/s. The temperature distribution on the metallic surfaces was monitored with the thermal camera, while the outlet water temperature was measured with thermocouples until no significant variations with time were observed, from which was possible to conclude that a steady state was reached after 110 s. The steady state temperature distribution at the tube and fins surface can be seen in Fig. 9. Three sampling points, P1, P2 and P3, were chosen as indicated on the surfaces of Fig. 9, and their temperatures extrapolated from the available scale of the calibrated thermal camera. The position of these three measurement points was selected to minimize the possible distortion of infrared radiation and thus achieve better accuracy.

To mimic the same configuration reported in Fig. 9, a numerical CFD model was built with a domain composed by the finned tube and a water volume flowing inside the tube. The different materials were defined with their thermophysical properties. A boundary

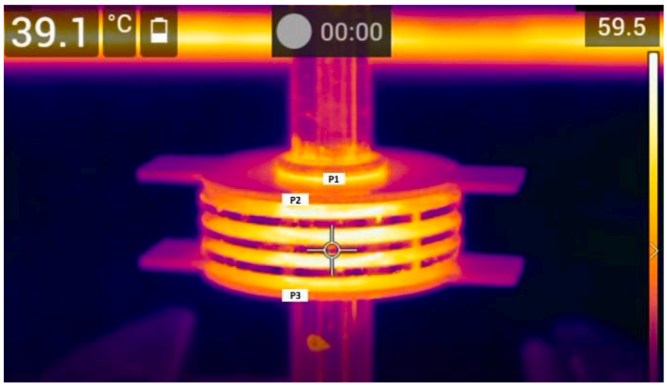

Fig. 9. Temperature distribution on the tested prototype surface, as experimentally obtained from the thermal camera. The three sampling temperature points are highlighted.

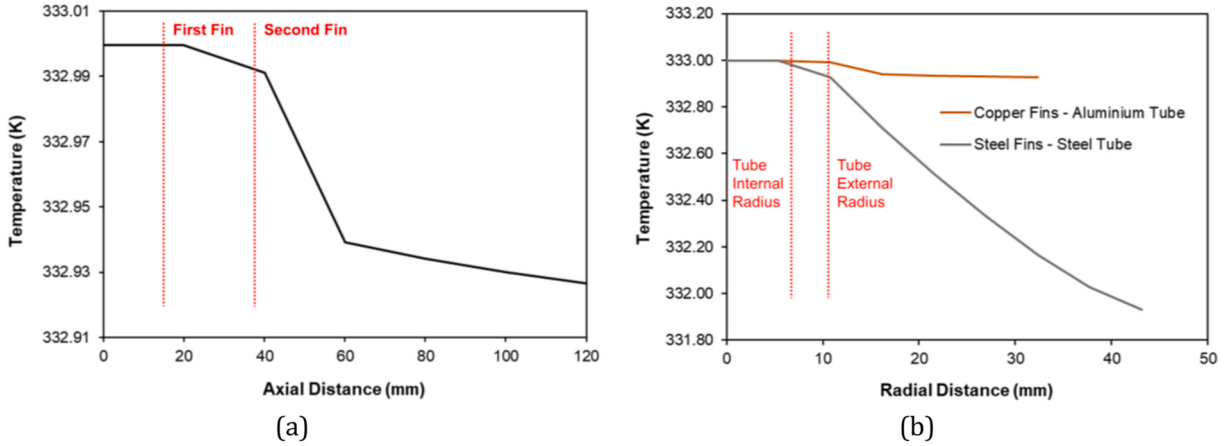

Fig. 10. Distribution of temperature (a) along line 1 and (b) along lines 2 and 3 of Supplementary Fig. S4.

condition of '*mass-flow inlet*' was assigned to the inlet surface, an '*outflow*' condition to the outlet surface, and a '*convection*' condition on all the external tube and fins surface exposed to the ambient air. A free stream temperature of 28 °C (the measured room air temperature) and a convection coefficient of 5 W/m^{2}K were chosen. The latter is a typical value for natural convection over vertical walls.

In Supplementary Table S1, the temperature values from the experimental test are compared with those obtained numerically for P1, P2, and P3 and the outlet water temperature. A good matching between experimental and numerical temperature fields can be observed. In fact, comparing the temperature values from the thermal camera and the simulation output, differences lower than 0.5 % can be noticed for the three sampling points considered.

Once the reliability of the numerical results was assessed, a deeper numerical analysis was carried out to obtain better insights on the temperature distribution throughout the prototyped heat exchanger. Three axes were defined in the model (see Line 1, 2 and 3 in Supplementary Fig. S4) and the temperature distribution along them evaluated. Line 1 allows to depict the distribution of water temperature along the tube axis, whereas Lines 2 and 3 show the temperature distribution along the radial direction in the middle of the central copper fin and of the last steel fin, respectively. In Fig. 10a, the temperature distribution along line 1 is plotted. The decrease of water temperature is quantitatively small from the tube inlet ($z = 0$ mm) to outlet ($z = 120$ mm), since the heat exchanged with the ambient air in natural convection is limited. However, a clear slope change in the temperature distribution is visible in correspondence of the fins, where the greatest part of heat is exchanged. Fig. 10b highlights the different thermal behaviour of copper and steel fins. The temperature remains almost constant for a radial distance smaller than the internal radius of the tube, due to the forced convection of the inner water. With larger radial distances, the differences in the temperature distribution become more noticeable because of the different fin efficiency of steel and copper fins, again validating the importance of an appropriate choice of materials in finned heat exchangers.

4. Conclusions

The use of joining by forming to create finned tube heat exchangers through axial tube compression at ambient temperature enhances performance by enabling the integration of dissimilar materials such as aluminium tubes, copper fins, and steel shells with minimal thermal contact resistance. This innovative joining technology, which is a viable alternative to traditional welding, offers considerable advantages including high repeatability, shorter production times, and elimination of thermal cycles that could induce residual stresses at the junctions of tubes and fins. It is also capable of joining dissimilar materials and it is cost-efficient, since it eliminates the need for filler materials, shielding gases and specialized operators.

In this study, a finned heat exchanger utilizing this method was developed and examined, marking a first in the research. The design process combined parametric CFD simulations for optimal tube-fin layout and finite element modeling to predict deformation mechanisms. The numerical simulations, experimentally validated, demonstrated a potential 108 % increase in heat transfer rate and doubled effectiveness compared to conventional all-steel designs, along with a 5 % reduction in weight.

Although the current continuum models have been preliminary explored, further investigation is necessary to broaden the range of parameters assessed and to pursue global design optimization. Looking ahead, these multi-material finned heat exchangers could be pivotal in applications such as thermal energy storage [21], electronics cooling [22], industrial [23], and building thermal systems [24].

CRediT authorship contribution statement

Riccardo Saltarelli: Writing – review & editing, Visualization, Validation, Software, Methodology, Investigation, Formal analysis. **Luís M. Alves:** Writing – review & editing, Supervision, Methodology, Investigation, Formal analysis. **Matteo Fasano:** Writing

– review & editing, Supervision, Methodology, Investigation, Formal analysis. **Rafael M. Afonso:** Writing – original draft, Visualization, Supervision, Resources, Project administration, Methodology, Investigation, Formal analysis, Conceptualization.

Declaration of competing interest

The authors declare that they have no known competing financial interests or personal relationships that could have appeared to influence the work reported in this paper.

Data availability

Data will be made available on request.

Acknowledgments

The authors acknowledge Fundação para a Ciência e a Tecnologia (FCT) for its financial support via the projects LAETA Base Funding (DOI: 10.54499/UIDB/50022/2020) and LAETA Programmatic Funding (DOI: 10.54499/UIDP/50022/2020). An acknowledgement is provided to Prof. Paulo A.F. Martins for the development of the i-form software.

Appendix A. Supplementary data

Supplementary data to this article can be found online at https://doi.org/10.1016/j.csite.2024.104551.

References

[1] T. Keawkamrop, M. Mesgarpour, A.S. Dalkılıç, H.S. Ahn, O. Mahian, S. Wongwises, Effect of the segmented fin height on the air-side performance of serrated welded spiral fin-and-tube heat exchangers, Case Stud. Therm. Eng. 35 (2022) 102128, https://doi.org/10.1016/j.csite.2022.102128.
[2] M. Sajawal, T.U. Rehman, H.M. Ali, U. Sajjad, A. Raza, M.S. Bhatti, Experimental thermal performance analysis of finned tube-phase change material based double pass solar air heater, Case Stud. Therm. Eng. 15 (2019) 100543, https://doi.org/10.1016/j.csite.2019.100543.
[3] L. Ventola, G. Curcuruto, M. Fasano, S. Fotia, V. Pugliese, E. Chiavazzo, P. Asinari, Unshrouded Plate fin heat sinks for electronics cooling: validation of a comprehensive thermal model and cost optimization in semi-active configuration, Energies 9 (2016) 608, https://doi.org/10.3390/en9080608.
[4] J. García González, J.J. Hernández-Ortega, A.-E. Jiménez-Ballesta, R.Z. Pedreño, Analysis of tube-to-tube sheet welding in carbon steel heat exchangers of a double plate header box, Materials 15 (2022) 261, https://doi.org/10.3390/ma15010261.
[5] P. Kiatpachai, T. Kaewkamrop, M. Mesgarpour, H.S. Ahn, A.S. Dalkılıç, O. Mahian, S. Wongwises, Air-side performance of embedded and welded spiral fin and tube heat exchangers, Case Stud. Therm. Eng. 30 (2022) 101721, https://doi.org/10.1016/j.csite.2021.101721.
[6] H. Han, L. Yang, J. Jiang, J. Ma, Experimental investigations of expansion strength of hydraulic expansion joints interconnecting tube and fins heat exchanger, Metals 12 (2022) 641, https://doi.org/10.3390/met12040641.
[7] H. Ma, H.J. Yu, C.F. Qian, Z.S. Liu, J.X. Zhou, Experimental study of hydraulic expanded tube-to-tubesheet joints for shell-and-tube heat exchangers, Procedia Eng. 130 (2015) 263–274, https://doi.org/10.1016/j.proeng.2015.12.220.
[8] K.P. Singh, A.I. Soler, Tube-to-Tubesheet joints, in: Mechanical Design of Heat Exchangers, Springer, Berlin, 1984, pp. 307–386, https://doi.org/10.1007/978-3-662-12441-3_7.
[9] M. Avalle, A. Scattina, Experiment based modeling of the mechanical expansion of tubes for the construction of heat exchangers, Procedia Struct. Integr. 12 (2018) 130–144, https://doi.org/10.1016/j.prostr.2018.11.100.
[10] A.S. Alaboodi, Finite element study of the hybrid expansion of tube-to-tubesheet joints, Thin-Walled Struct. 137 (2019) 347–352, https://doi.org/10.1016/j.tws.2019.01.025.
[11] L.M. Alves, R.M. Afonso, P.A.F. Martins, A new deformation assisted tube-to-tubesheet joining process, Thin-Walled Struct. 163 (2021) 107784, https://doi.org/10.1016/j.tws.2021.107784.
[12] L.M. Alves, R.M. Afonso, F.L.R. Silva, P.A.F. Martins, Deformation-assisted joining of sheets to tubes by annular sheet squeezing, Materials 12 (2019) 3909, https://doi.org/10.3390/ma12233909.
[13] L.M. Alves, R.M. Afonso, P.A.F. Martins, A new deformation assisted joining process for connecting tubes to stronger tubesheets, Thin-Walled Struct. 173 (2022) 108975, https://doi.org/10.1016/j.tws.2022.108975.
[14] L.M. Alves, T.J. Reis, R.M. Afonso, P.A.F. Martins, Single-stroke attachment of sheets to tube ends made from dissimilar materials, Materials 14 (2021) 815, https://doi.org/10.3390/ma14040815.
[15] L.M. Alves, E.J. Dias, P.A.F. Martins, Joining sheet panels to thin-walled tubular profiles by tube end forming, J. Clean. Prod. 19 (2011) 712–719, https://doi.org/10.1016/j.jclepro.2010.12.014.
[16] D. Van Heerden, T.R. Rude, J. Newson, J. He, E. Besnoin, O.M. Knio, T.P. Weihs, A tenfold reduction in interface thermal resistance for heat sink mounting, Journal of Microelectronics and J. Microelectron.Electron.Packag. 1 (2004) 187–193.
[17] P. Asinari, M. Fasano, E.A. Chiavazzo, Kinetic perspective on k–ε turbulence model and corresponding entropy production, Entropy 18 (2016) 121, https://doi.org/10.3390/e18040121.
[18] A. Ciuffini, A. Scattina, F. Carena, M. Roberti, G. Toscano Rivalta, E. Chiavazzo, M. Fasano, P. Asinari, Multiscale computational fluid dynamics methodology for predicting thermal performance of compact heat exchangers, J. Heat Tran. 138 (2016) 071801, https://doi.org/10.1115/1.4032980.
[19] Y.A. Cengel, Introduction to Thermodynamics and Heat Transfer, vol. 846, McGraw-Hill, New York, 1997.
[20] C.V. Nielsen, W. Zhang, L.M. Alves, N. Bay, P.A.F. Martins, Coupled finite element flow formulation, in: Modeling of Thermo-Electro-Mechanical Manufacturing Processes, Springer, London, 2013, pp. 11–36, https://doi.org/10.1007/978-1-4471-4643-8_3.
[21] M. Morciano, M. Alberghini, M. Fasano, M. Almiento, F. Calignano, D. Manfredi, P. Asinari, E. Chiavazzo, 3D printed lattice metal structures for enhanced heat transfer in latent heat storage systems, J. Energy Storage 65 (2023) 107350, https://doi.org/10.1016/j.est.2023.107350.
[22] L. Ventola, M. Dialameh, M. Fasano, E. Chiavazzo, P. Asinari, Convective heat transfer enhancement by diamond shaped micro-protruded patterns for heat sinks: thermal fluid dynamic investigation and novel optimization methodology, Appl. Therm. Eng. 93 (2016) 1254–1263, https://doi.org/10.1016/j.applthermaleng.2015.10.065.
[23] F. Cola, M. De Gennaro, D. Perocchio, E. Canuto, S. Daniele, P. Napoli, G. Toscano Rivalta, E. Chiavazzo, M. Fasano, P. Asinari, Integrated receivers with bottom subcooling for automotive air conditioning: detailed experimental study of their filling capacity, Int. J. Refrig. 62 (2016) 72–84, https://doi.org/10.1016/j.ijrefrig.2015.08.021.
[24] S.F. Ahmed, M. Khalid, M. Vaka, R. Walvekar, A. Numan, A.K. Rasheed, N.M. Mubarak, Recent progress in solar water heaters and solar collectors: a comprehensive review, Therm. Sci. Eng. Prog. 25 (2021) 100981, https://doi.org/10.1016/j.tsep.2021.100981.